Interactions between methanol/toluene binary mixtures and an organic solvent nanofiltration PIM-1 membrane

M.-L. Ouinten, Anthony Szymczyk, Aziz Ghoufi

Version of Record: https://www.sciencedirect.com/science/article/pii/S0167732222006845
Manuscript_36339fa2d63f0f69a012685b82395f0b

Interactions between Methanol/Toluene Binary Mixtures and an Organic Solvent Nanofiltration PIM-1 Membrane

Mohammed-Lamine Ouinten

Institut de Physique de Rennes, IPR, CNRS-Université de Rennes 1, UMR CNRS 6251, 35042 Rennes, France

Univ Rennes, CNRS, ISCR (Institut des Sciences Chimiques de Rennes) - UMR 6226, F-35000 Rennes, France

Anthony Szymczyk*

Univ Rennes, CNRS, ISCR (Institut des Sciences Chimiques de Rennes) - UMR 6226, F-35000 Rennes, France

Aziz Ghoufi**

Institut de Physique de Rennes, IPR, CNRS-Université de Rennes 1, UMR CNRS 6251, 35042 Rennes, France

Abstract

In this work, a molecular scale study of the interactions between a polymer with intrinsic microporosity (PIM-1) membrane and toluene, methanol and their mixtures was performed by means of molecular dynamics simulations. From the radial distribution functions we highlight specific interactions between the hydroxyl group of methanol and the aromatic ring of toluene as well as with the PIM-1 membrane. Moreover, the presence of nitrogen atoms on the PIM-1 backbone makes it possible the formation of hydrogen bonds like interaction (close contact of 2.5 Å) between the methanol molecules and the PIM-1 membrane, thus leading to interfacial anchoring of methanol at the polymer surface and moving toluene molecules away from the surface. However

*Corresponding author
**Corresponding author
Email addresses: anthony.szymczyk@univ-rennes1.fr (Anthony Szymczyk), aziz.ghoufi@univ-rennes1.fr (Aziz Ghoufi)

some toluene molecules are located around 3.5 Å due to π-stacking interaction between the aromatic rings of the PIM-1 membrane and those of the confined TOL molecules. At short range, the confined methanol molecules interact with each other like their bulk-phase counterparts whereas long range correlations highlight a existence of confined methanol aggregates. The specific interactions between toluene, methanol and the PIM-1 membrane result in a linear increase of the membrane swelling with the mole fraction of toluene in the binary mixtures.

Keywords: PIM-1, interactions, molecular simulation, structure

2010 MSC: 00-01, 99-00

---

1. Introduction

Nowadays membrane processes are considered as a key technology for sustainable processes and green engineering developments [1]. Membrane processes require highly selective materials, capable of discriminating between solutes of different molecular sizes and/or physicochemical properties. Their use for processing organic fluids remains relatively unexplored when compared to water purification and gas separations, largely due to the difficulty in developing membrane materials that are both stable and scalable [2]. The so-called organic solvent nanofiltration (OSN) process has emerged in the early 2000s with the development of polymer membranes with improved resistance towards organic solvents [3]. In OSN, separations down to the molecular level can be realized in solvent streams by simply applying an external pressure over a solvent-resistant membrane. OSN has been regarded in recent years as a separation technique with a very high potential and pioneering works have highlighted its high potentiality in petrochemical [4] and pharmaceutical industries [5] as well as for catalytic applications [6] because of the numerous advantages it offers in terms of purification, disposal of pollutants, environmental footprint and energy savings.

The relatively low manufacturing cost of polymer membranes together with the easy processing of large-area membranes have led to the dominant posi-

tion of polymer membranes worldwide. However, the lack of solvent-resistant membrane materials was for a long time the major bottleneck for systematic research on OSN. Indeed, polymer membranes, which were originally developed for applications in aqueous phase (e.g. seawater desalination), loose their stability and/or provide poor flux/rejection performance in many organic solvents. Moreover, in OSN the non woven backing material have to be solvent resistant and should ideally behave the same way as the polymer membrane (i.e., have a similar degree of swelling) to avoid the formation of creases, which could lead to membrane failure. Recent advances in the synthesis of solvent-resistant membranes have made it possible to overcome (at least to some extent) this bottleneck. Notably, polyimide (PI) and polydimethylsiloxane (PDMS) membranes have been shown to exhibit quite good chemical resistance in many commonly organic solvents (acetone, toluene, hexane...) and are currently the most used membranes in OSN applications. Novel coating materials, known as polymers with intrinsic microporosity (PIM-1) and characterized by ultrahigh free volume, have also been proposed recently as possible candidates for OSN applications. Indeed, membranes built of PIM-1 showed high permeance in apolar solvents and alcohols, in comparison with commercial polyimide membranes [7].

However, despite the numerous advantages of OSN in terms of sustainability, the development of new applications proceeds slowly due to an additional bottleneck related to the lack of knowledge and understanding of the mechanisms controlling the membrane performance (flux and rejection) in non-aqueous media. Solvent sorption and related effects such as membrane swelling as well as the solvent–membrane affinities have a dramatic influence on both flux and rejection [8, 9, 10]. Livingston and coworkers conducted a systematic comparison of different transport models (irreversible thermodynamics, solution-diffusion, pore-flow and transient transport models) for OSN, and highlighted the applicability of each model [11]. It was suggested that at least three factors, namely the solvent viscosity, surface tension and dielectric constant should be taken into account for evaluating OSN performance. However, such a correlation was not found for the permeations of methanol, toluene and n-heptane through an

oxidized poly(arylene sulfide sulfone) membrane, and was ascribed to the interaction between solvent and membrane [12]. Therefore, the way organic solvents interact with and permeate through polymer membranes is not straightforward. Many complex factors come into play to govern OSN performance and their quantitative effects remain elusive. These few examples underline the complexity of the molecular mechanisms ruling separations in non-aqueous media, which result from intermolecular interactions between the membrane material, the solvent and the solute(s).

The above-mentioned examples taken from recent literature highlight the limits of existing theoretical models in terms of fundamental understanding of the molecular mechanisms involved in OSN and the need to develop new approaches allowing the rationalization of the underlying physical phenomena. Indeed, as a result of the lack of understanding of the molecular mechanisms controlling membrane performance in OSN, decisions regarding the selection of a suitable membrane/solvent (or solvent mixture) system for a given application are currently taken based on costly and time-consuming screening experiments, thus slowing down the development of new OSN applications considerably and impairing the overall sustainability of the process. In order to go one step further in the understanding of OSN it is important to keep in mind that separations by OSN polymer membranes occur inside free volume elements that are no larger than a few angstroms.

Consequently, modeling OSN membranes at the molecular scale is highly desirable in order to rationalize experimental observations and gain a deeper insight into the molecular mechanisms ruling solvent and solute permeation that are connected to the molecular interactions between solvents and polymers. Therefore a prerequisite to well apprehend the solvent transport through OSN membrane is the fine molecular characterization of solvent/membrane interactions. With the tremendous advance of computational power, molecular simulation has increasingly become a robust tool in materials science and engineering. Indeed, simulation at a molecular scale can provide microscopic pictures that otherwise are experimentally inaccessible or difficult to obtain, and thus eluci-

date the underlying physics from bottom-up. Molecular insights gained from simulation can also assist in the characterization and rational design of new materials for emerging applications. Recently a molecular simulation protocol has been developed to investigate the swelling of PIM-1 in methanol, ethanol, acetonitrile and acetone and to examine the OSN through the swollen membranes [13, 9, 14]. The simulation protocol was found to simulate membrane swelling quite efficiently. The predicted swelling degrees of membranes, the polymer-solvent solubility parameter differences, the mean pore sizes of swollen membranes and the predicted solvent permeabilities through PIM-1 membranes have been found in fair concordance with experimental data. Liu et al. have also examined polymer-solvent interaction through the calculation of solvent-PIM1 binding energy [9]. In a more recent work, the solvent permeabilities were connected to favorable interactions with protic solvents and preferential sites of adsorption, pore size distribution and swelling rate [13, 10], and interaction energies of solute with membrane and solvent was investigated and connected the transport properties. However, the structural organization and hydrogen bonding network of protic solvent were not examined. Furthermore, binary liquid mixtures separation have never been investigated from atomistic simulation.

Among most popular filtered solvents, methanol and toluene are often considered as the most simple models to examine both polar and apolar interactions. Furthermore, their mixtures in bulk phase are miscible and non-ideal, inducing localized microstructure [15]. Additionally, separation of a binary mixture containing methanol/toluene is a tough task because toluene forms azeotrope with methanol. An energy-efficient process such as OSN could then be very interesting to bypass the problem linked to the azeotrope. On top of that, methanol is often used to examine physical aging of polymer with intrinsic microporosity [16, 17, 18]. Understanding of PIM-1/Methanol interactions is then fundamental to well apprehend the microscopic mechanisms occurring during soaking of PIM-1 from methanol [19]. Additionally, although adsorption of methanol and toluene vapors and liquids through PIM-1 has been examined in terms of swelling [20], confinement of pure methanol and toluene liquids has been much

less studied [21, 9, 10] and confinement of methanol/toluene mixtures has never been investigated. In this study, we purpose to study confinement of toluene, methanol and their mixtures into a PIM-1 organic solvent nanofiltration membrane by means of molecular dynamics (MD) simulations to investigate the liquid/liquid and liquid/polymer intermolecular interactions. The structure of the confined liquids as well as that of the PIM-1 membrane was also examined as a function of the toluene/methanol uptake.

2. Methodology

3. METHODOLOGY

3.1. Polymer generation

The construction of the PIM-1 membrane was performed by means of the *in silico* polymerization approach developed by Abbot et al. and implemented in the Polymatic code [22] using LAMMPS[23] as MD package. It has been established that this methodology is suited for building amorphous polymer backbones, such as PIM-1 [24, 22]. As shown in Figure 1a and Figure 1b, the PIM-1 repeat unit contains two rigid parts connected by a twisted spiro-carbon. 230 repeat units were randomly inserted into a simulation box of dimensions 40x40x150 Å. We mainly followed the methodology proposed by Larsen et al. [24]. The equilibration of the simulation box containing the 230 repeat units was performed from an MD simulation of 5 ns in the NVT statistical ensemble (N, V and T are the number of particles, the volume and the temperature, respectively) at T=300 K followed by an MD run of 5 ns in the NpT statistical ensemble (p is the pressure) at T = 300 K and p = 1 bar.

A further step after the polymerization consisted in "capping" the so-generated polymer in order to avoid unphysical artifacts due to the presence of high-energy sites. For this purpose, Larsen et al. used neutral steric blocking groups [24]. Here, a more realistic "capping" was considered, consisting in the addition of H atoms to mimic the scenario in play for the experimentally synthesized polymer [25]. The polymerization resulted in a polydisperse mixture with chains ranging

from 2 to 52 monomers. Chains containing less than 16 monomers were removed and the membrane was then formed by 5 chains containing between 16 and 52 repeat units, which is close to the PIM-1 molecular model obtained by Larsen et al. [24].

The PIM-1 membrane was then equilibrated using the 21 MD-step scheme proposed by Hofmann et al. [26]. Seven cycles of three MD simulations each (1: NVT at T=600 K; 2: NVT at T=300K and 3: NpT at T=300K) were performed (details for each step are provided in Table 1). The pressure in the NpT simulations was gradually increased to reach $p_{max} = 50$ kbar in the third cycle and was further reduced stepwise in the subsequent cycles until it reached the final value of p = 1 bar. Figure 1c shows the final configuration of the PIM-1 membrane after this 21-step relaxation process and highlights the nanoporous domains. Final box dimensions of dry PIM-1 membrane are L_x=L_y=41.2 Å and L_z=82.4 Å where L_x, L_y are L_z are box lengths according to x, y, and z directions.

3.2. Force Field and computational procedure

PIM-1 was described using a united-atom description (see Figure 1b). Each CHx (x=1,2,3) group of the membrane was considered as a single particle (the united-atom approach (UA)) to reduce the simulation time. Let us note that the hydrogen atoms on methyl groups do not impact polar interactions such as hydrogen bonds. Furthermore, the steric hindrance induced by methyl groups is well taken into account from UA models. The energy of the system was described as the sum of bonded and non-bonded contributions. The former includes harmonic potentials to model the stretching and bending modes, as well as cosine-based functions for dihedrals and improper dihedrals torsions. The force-field parameters for the PIM-1 membrane were obtained from the GAFF force field [27], which proved to reproduce well the structural properties of the PIM-1 polymer [28, 29]. Toluene (TOL) and methanol (MeOH) molecules were described by the OPLS all-atoms force field [30] that well reproduced the thermodynamics properties of the MeOH/TOL mixtures [15]. The partial charges on

Table 1: Details of the thermodynamic conditions for the 21 MD steps implemented to relax the PIM-1 membrane.

Step	ensemble	T (K)	p (kbar)	Time (ps)
1	NVT	600		50
2	NVT	300		50
3	NpT	300	1	50
4	NVT	600		50
5	NVT	300		100
6	NpT	300	30	50
7	NVT	600		50
8	NVT	300		100
9	NpT	300	50	50
10	NVT	600		50
11	NVT	300		100
12	NpT	300	25	5
13	NVT	600		5
14	NVT	300		10
15	NpT	300	5	5
16	NVT	600		5
17	NVT	300		10
18	NpT	300	0.5	5
19	NVT	600		5
20	NVT	300		10
21	NpT	300	0.001	2000

the various atoms of the PIM-1 membrane were taken from Ref. [29]. The TOL and MeOH molecules were randomly inserted into the PIM-1 membrane with

a distance criterion of 2.5 Å. An energy minimization and a 10 ns equilibration in the NPT statistical ensemble were further performed. Eleven molar fractions were considered from x_{MeOH}=0.0 (pure TOL) to x_{MeOH}=1 (pure MeOH). The total number of molecules was determined based on the experimental density of confined pure TOL and MeOH [7]. The number of inserted molecules as well as the corresponding molar fractions are provided in Table 2. Three configurations were considered and similar swelling and structural properties were found, thus suggesting that our results are independent of the initial state. To ensure that the PIM-1 membrane was correctly filled, additional simulations with explicit polymer/liquid interfaces were performed. For this purpose, graphitic walls were used as pistons to push the TOL and MeOH molecules into the PIM-1 membrane (see Figure 1d). [31]. Methodological details of simulations can be found elsewhere [32]. Three molar fractions of MeOH (x_{MeOH}=0.25, 0.50 and 0.75) in the reservoirs were considered. From 20 ns simulations, the molar fractions of MeOH in the membrane obtained from these simulations with explicit interfaces (x^{ei}_{MeOH}) were found very close to the molar fractions outside the membrane (see Table 2) and the numbers of TOL and MeOH molecules in the membrane were found in fair agreement with the number of molecules inserted in the membrane for the simulations performed without explicit interfaces.

The interactions between PIM-1, TOL and MeOH were taken as a combination of electrostatic and van der Waals (VdW) interactions. The VdW contributions were modeled by considering Lennard-Jones potentials. The cross-interactions were calculated by means of the Lorentz-Berthelot mixing rules. The electrostatic interactions were computed from the Ewald sum method [33, 34]. All interactions were truncated by using a cutoff of 12 Å. Simulations were performed using the LAMMPS package [23]. The velocity Verlet propagator combined with the Nose-Hoover thermostat and barostat were considered [35]. Relaxation times of 0.5 ps were used for both the thermostat and barostat. The acquisition phase was conducted over the last 20 ns of the simulation after a 50 ns equilibration stage and with a timestep of 1 fs. Periodic boundary conditions were applied in the three directions. The analysis of the membrane pore size

Table 2: Methanol molar fractions (x_{MeOH}) and numbers of methanol (N(MeOH)) and toluene (N(TOL)) molecules inserted into the PIM-1 and number of molecules ($N(TOL)^{ei}$, $N(MeOH)^{ei}$) and methanol molar fractions (x^{ei}_{MeOH}) in the membrane for simulations performed with explicit interfaces.

x_{MeOH}	N(Tol)	N(MeOH)	$N(Tol)^{ei}$	$N(MeOH)^{ei}$	x^{ei}_{MeOH}
0	1200	0	-	-	-
0.1	1080	120	-	-	-
0.2	960	240			
0.25	900	300	731	256	0.26
0.3	840	360	-	-	-
0.4	720	480	-	-	-
0.5	600	600	558	543	0.49
0.6	480	720	-	-	-
0.7	360	840			
0.75	300	900	352	1003	0.74
0.8	240	960	-	-	-
0.9	120	1080	-	-	-
1	0	1200	-	-	-

distribution (PSD) revealed a wide distribution with pore diameters ranging from 2 Å to 12 Å (Figure 1e). For the calculation of the pore size distribution, we used the zeo++ software [36] based on the Voronoi decomposition, which provides a graphic representation of the void space for a given arrangement of atoms in a periodic domain. The resulting Voronoi network was analyzed to obtain the diameter of the largest included sphere and the largest free sphere, which are two geometrical parameters that are frequently used to describe pore

geometry. The average pore diameter was found around 7.1 Å , which is in fair agreement with experiment as values between 7 Å and 10 Å have been reported [37, 38]. Furthermore, the density of the PIM-1 membrane molecular model was found to be 1157.8 ± 1.9 kg/m^3, which is close to the experimental value of 1092 kg/m^3 [39]. These fair agreements with experiments validate the force field and the methodology followed to develop our PIM-1 molecular model.

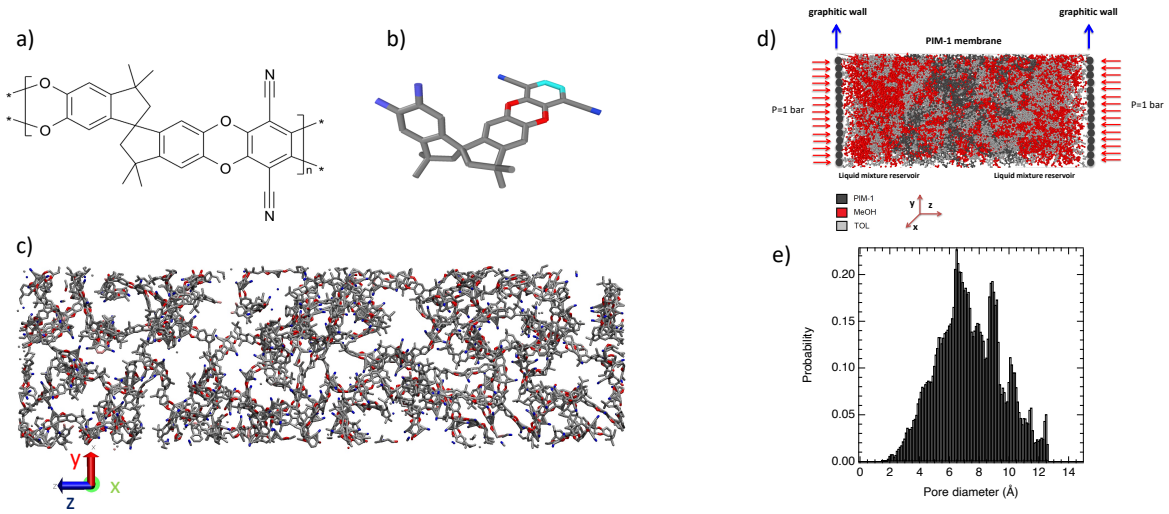

Figure 1: a) Chemical structure of the PIM-1 repeat unit. b) United-atom model used in MD simulations. Grey, red and blue colors correspond to carbon, oxygen and nitrogen atoms, respectively. The atoms in cyan color represent carbon atoms allowing the connection with two repeat units. c) Illustration of a simulation with explicit polymer/liquid interfaces. Red arrows indicate the applied force on the graphitic walls (leading to a pressure of 1 bar. d) Final relaxed PIM-1 polymer configuration after the virtual polymerization and relaxation process described in Table 1. e) Pore size distribution of the dry PIM-1 membrane at T=300 K and p=1 bar.

4. Results and Discussion

Figure 2a shows the volume of the PIM-1 membrane as a function of x_{MeOH}. The uptake of TOL and MeOH induces a structural modification of the membrane. Indeed, a gradual membrane swelling is observed when the liquid com-

position is varied from x_{MeOH}=1 (pure MeOH) to x_{MeOH}=0 (pure TOL) with a linear volume decrease for increasing x_{MeOH} values. The theoretical volume (V_{Dry}+N(MeOH)V(MeOH) + N(TOL)V(TOL), with V(MeOH), V(TOL), N(MeOH) and N(TOL) the molecular volumes and molecule numbers of MeOH and TOL) was calculated and reported in Figure 2a. The system was found to exhibit a deviation from the theoretical behavior, thus suggesting additional physical effects responsible for swelling. We determined the excess molar volume ($V^x = (x_{MeOH} * M_{MeOH} + x_{TOL} * M_{TOL})/\rho^{mix} - (x_{MeOH} * M_{MeOH}/\rho^{MeOH} + x_{TOL} * M_{TOL}/\rho^{TOL}$) where ρ^*_{MeOH} and ρ^*_{TOL} are the density of pure MeOH and TOL confined in PIM-1 while M_{MeOH} and M_{TOL} correspond to the molar mass of each component. ρ^{mix} and ρ^{MeOH} represent the simulated and the ideal densities, respectively) as a function of the MeOH molar fraction.

As shown in Figure 2b, the excess molar volume was found negative, which can be ascribed to specific interactions between TOL, MeOH and PIM-1 leading to modification of the Hydrogen-bond network. The increase in the PIM-1 membrane volume was found to be 103 % and 34 % when the membrane was filled with pure TOL and pure MeOH, respectively. This large variation of membrane swelling results from (i) the larger size of TOL (5.7 Å) than MeOH (4.0 Å) and (ii) the apolar TOL/TOL and TOL/PIM-1 interactions. Indeed, the apolar interactions increase the separation distance between the confined TOL molecules and the polymer, thus leading to the increase of the membrane volume. Calculating the preferential interaction parameter between the PIM-1s and solvent components have been then performed from radial distribution functions (noted RDF). RDF between the centres of mass (com) of aromatic rings of the TOL molecules (TOL/TOL) as well as between the com of aromatic rings of the PIM-1 membrane and those of the TOL molecules (TOL/PIM-1) were thus managed. RDF is a relevant tool in statistical mechanics to study the strength of interactions from the location of main peak.. As highlighted in Figure 2c the first peak of RDF between TOL molecules and PIM-1 is located around 3.5 Å. According to Figure 2c, the TOL/PIM-1 interactions are more favorable than the TOL/TOL interactions as the maximum of the first peak of the RDF between

the TOL aromatic rings was found at a much larger distance (around 6 Å). This shift is observed for the whole range of methanol fractions and can be explained by π-stacking between the aromatic rings of the PIM-1 membrane forming an aromatic ring chain and those of the confined TOL molecules as shown in Figure 2c. Interestingly, the TOL-TOL distance of the first peak in bulk phase (6.1 Å) is found at the same order of magnitude that in confined phase. This suggests that the position of the 1st peak is not determined by steric factors but rather by the strength of the interactions. To be sure that the smaller degree of swelling with MeOH than with TOL is not the result of the smaller volume of MeOH we carried out MD simulations of pure dicholoromethane confined in PIM-1. Indeed, CH_2Cl_2 and CH_3OH molecules have similar molecular diameter (4.2 Å vs 4.5 Å). CH_2Cl_2 was modeled as a rigid body by using the force field developed by Evans et al. [40] and by considering same number of MeOH molecules for x_{MeOH}=1. With CH_2Cl_2 an increase in the PIM-1 membrane volume of 67 % was found between TOL and MeOH. This result suggests that swelling is partially ruled by the strength of interactions between PIM-1 and solvent molecules.

We report in Figure 2d the RDF between the OH group of MeOH molecules and the center of mass of aromatic rings of TOL. The first peak is located at 2.5 Å , highlighting a hydrogen bond HB-like interaction between the aromatic ring of TOL and the hydrogen atom of the hydroxyl group of MeOH [41, 15]. This HB-like interaction between TOL and MeOH is probably at the origin of the miscibility of these two liquids [15]. Interestingly, Figure 2d shows a similar favorable interaction between the aromatic rings of the PIM-1 membrane and the hydrogen atom of the hydroxyl groups of MeOH.

Figure 3a shows that swelling results in a shift of the membrane pore size distribution with an increase in the average pore diameter of the solvated PIM-1 membrane from 7.1 Å for the dry membrane to 9.2 Å and 14 Å for the membrane filled with MeOH and TOL, respectively. To examine the connection between the chain flexibility and swelling the dihedral twisted spiro-carbon angle distribution of PIM-1 is reported in Figure 3b. Figure 3b shows that the dihedral

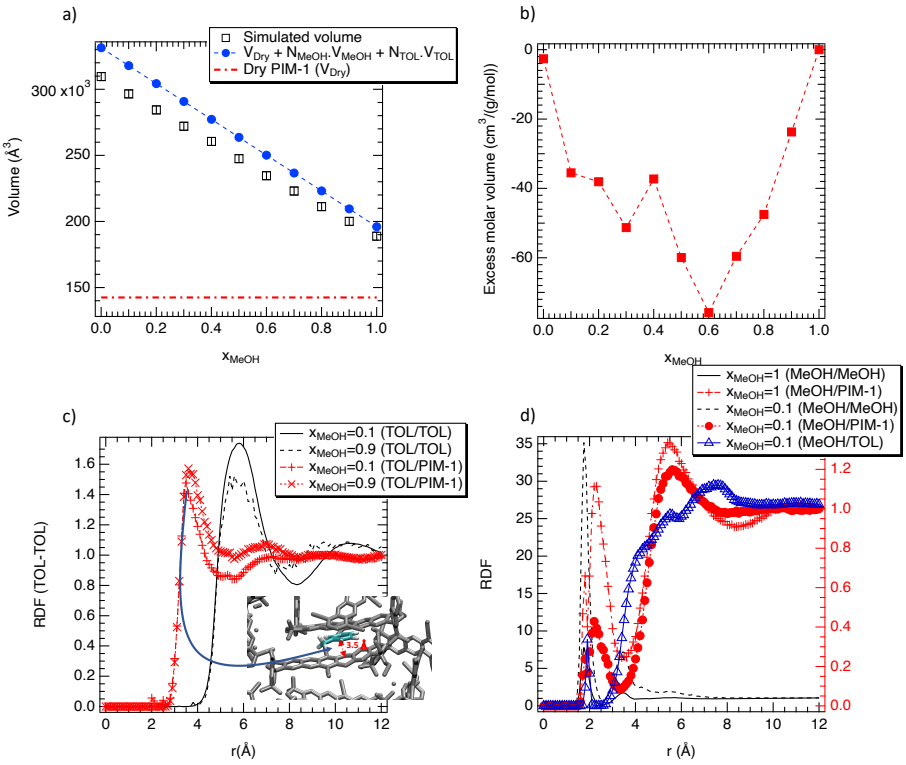

Figure 2: a) Volume of the PIM-1 membrane at T=300 K as a function of x_{MeOH}. The horizontal dashed line represents the volume of the dry PIM-1 membrane. b) Excess density as a function of x_{MeOH}. c) Radial distribution functions (RDF) between the centre of mass of the TOL molecules and between the TOL molecules and the PIM-1 aromatic rings. An illustration of the distance between both aromatic cycles is also provided such as gray color corresponds to the PIM-1 material. d) RDF between the hydrogen atom of the hydroxyl groups of MeOH and the PIM-1 aromatic rings (right axis) and between the oxygen atom of MeOH and the hydrogen atom of the hydroxyl groups of the other MeOH molecules (left axis).

angle distribution is similar for the whole range of MeOH fractions, which sug-
285 gests a similar flexibility of the swollen membranes [42]. Indeed, a predominant angular distribution was found but other configurations with smaller probability were also observed for the whole range of MeOH molar fractions, which suggests that the internal structure of PIM-1 was only slightly impacted despite the decrease in the membrane volume with increasing MeOH molar fractions.

This result highlights that the flexibility of PIM-1 is weakly impacted by the solvation.

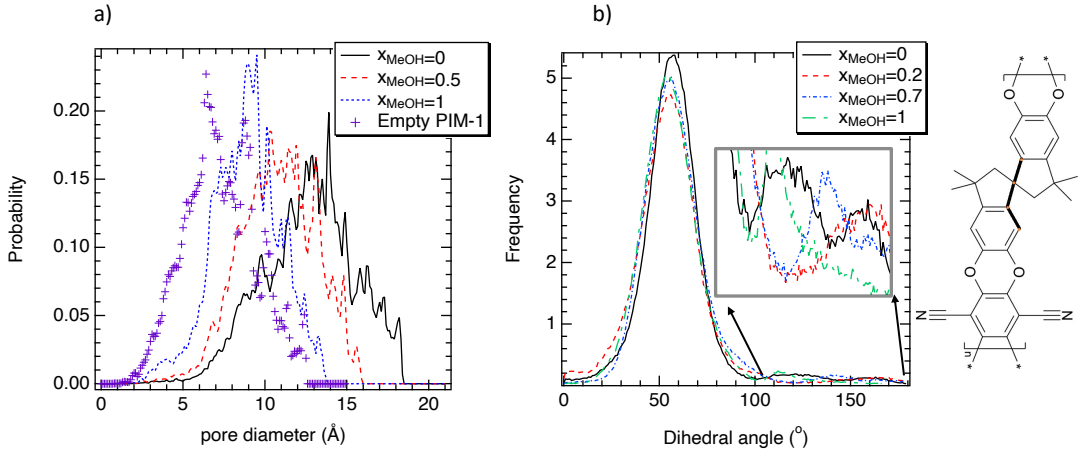

Figure 3: a) Pore size distribution of the PIM-1 membrane before and after swelling by liquids of various x_{MeOH}. b) Dihedral angle distribution of twisted spiro-carbon as a function of the methanol concentration. The angle is illustrated through the sketch showing the repetition unit of PIM-1.The insert in part b) correspond to an enlargement of the dihedral distribution between 100 ^{o} and 150 ^{o}.

Figure 4a shows the RDF between the hydrogen atom of the hydroxyl groups of MeOH and the electron-rich oxygen and nitrogen atoms of PIM-1. Strikingly, HB interactions are observed between MeOH and the nitrogen atoms of PIM-1 (main peak of the RDF located below 2 Å) whereas no favorable interactions occur with the oxygen atoms of PIM-1 (most probably due to steric hindrance with less accessibility to the PIM-1 oxygen atoms; see Figure 1a). The nitrogen atoms of PIM-1 are then preferential interaction sites for MeOH. As expected, Figure 4b shows no preferential interactions between the carbon atoms of TOL aromatic rings and the oxygen and nitrogen atoms of PIM-1.

The number of hydrogen bonds (nHB) per MeOH molecule is reported in Figure 5a. nHB was estimated by considering the geometric criteria established by Luzar and Chandler [41]. The number of HBs between MeOH molecules decreases with decreasing x_{MeOH} as a result of dilution. On the other hand,

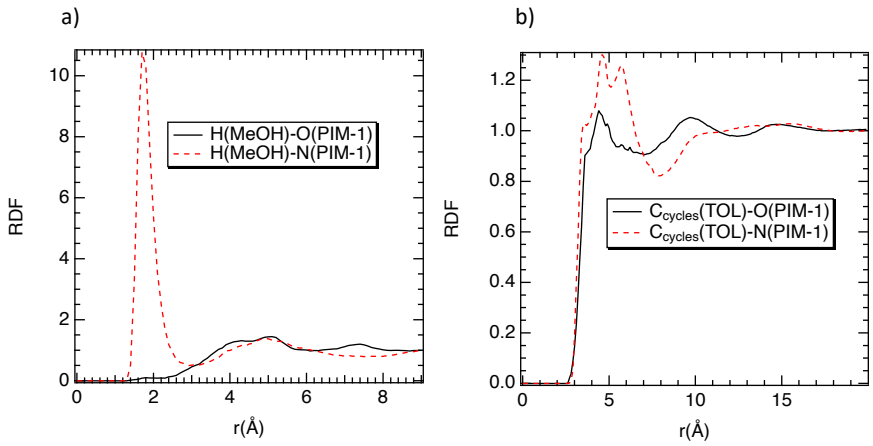

Figure 4: a) RDF between the hydrogen atom of the hydroxyl groups of MeOH and the oxygen and nitrogen atoms of PIM-1. b) RDF between the carbon atoms of the aromatic ring of TOL and the oxygen and nitrogen atoms of PIM-1.

the number of HBs between MeOH and the PIM-1 membrane increases when x_{MeOH} decreases because diluted MeOH molecules tends to compensate the decrease in MeOH/MeOH HBs by forming new HBs with the PIM-1 membrane. Interestingly, the total nHB (i.e. resulting from both MeOH-MeOH and MeOH-PIM-1 interactions) in the membrane phase is found very close to the number of HBs between MeOH molecules in the bulk phases, whatever the mixture composition (reaching 1.8 HB per MeOH molecule for x_{MeOH}=1.0). This finding suggests a limited impact of confinement by the PIM-1 matrix on the structure of MeOH at short range, which results from the rather large pores of the PIM-1 membrane (see Figure 3a). On the other hand, the microporosity of PIM-1 impacts the long-range structure of confined MeOH. Figure 5b shows the partial structure factor (S(Q), with Q the moment vector) between the oxygen and hydrogen atoms of different MeOH molecules. Details on the calculations of S(Q) can be found in Ref. [15]. As shown in Figure 5b, the main peak is shifted toward lower Q values when MeOH is confined in the PIM-1 membrane, which suggests long-range correlations between MeOH aggregates in the PIM-1 membrane. It is worth noting that the peak positions are not related to the cluster

size but rather to the range of interactions between aggregates [43].

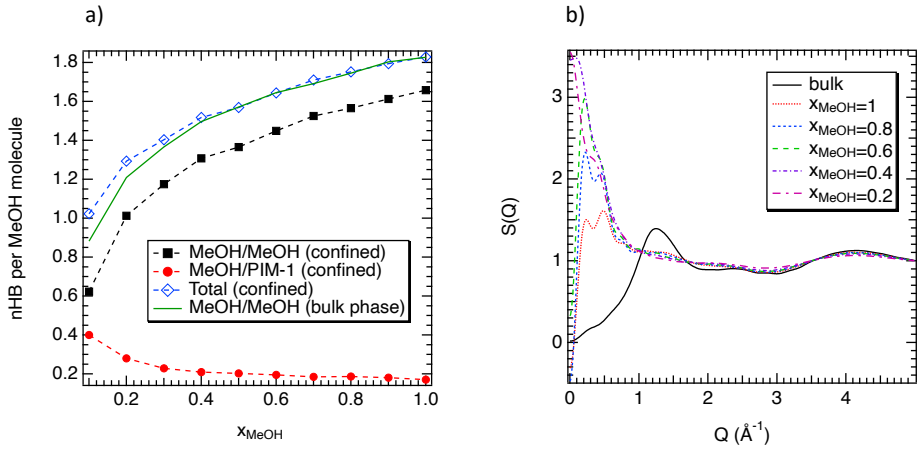

Figure 5: a) Number of hydrogen bonds (nHB) per MeOH molecule as a function of x_{MeOH}. b) Partial structure factor (S(Q)) between the oxygen and hydrogen atoms of different MeOH molecules for various x_{MeOH}.

We report in Figure 6 the number of MeOH clusters (from dimers to pentamers) in the various confined MeOH/TOL mixtures. The calculation of cluster size based on the hydrogen bonds was performed by considering the modified algorithm of Stoddard [44] using a distance criterion such that a cluster was considered if the molecules were within 3.5 Å of each other. At low x_{MeOH}, dimers and trimers were found predominant. The number of dimers and trimers first increased with x_{MeOH} and then slightly decreased for x_{MeOH} larger than 0.5 and 0.6, respectively. On the other hand, the number of larger clusters increased monotonously with x_{MeOH}. Overall, this result highlights the presence of clusters of different sizes induced by the microporosity of the PIM-1 membrane. Interestingly, Figure 6 shows that the number of the various clusters in the confined medium follows the same trend with the MeOH molar fraction as in the bulk phase. It is worth noting, however, that clusters made of more than five molecules were not found in the membrane due to restricted free volumes, contrary to the bulk phase where larger clusters (hexamers, heptamers and octamers) can be found [15].

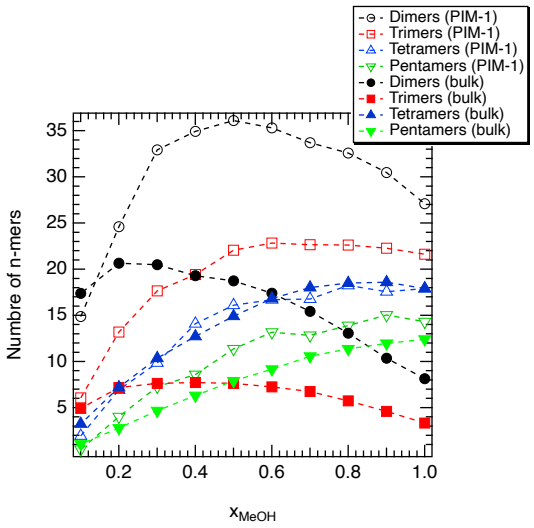

Figure 6: Number of MeOH clusters as a function of the MeOH molar fraction in PIM-1 material (empty symbols) and in bulk phase (filled symbols)

5. Conclusion

Molecular dynamics simulations of methanol/toluene mixtures confined in a PIM-1 organic solvent nanofiltration (OSN) membrane were performed. The density and the pore size distribution of the PIM-1 membrane molecular model were found in good agreement with reported experimental data. The structure of the PIM-1 membrane was examined as a function of the mixture composition. The PIM-1 membrane was found to swell to a larger extent in toluene than in methanol, which was shown to result from apolar interactions between toluene and the membrane while more favorable interactions between methanol and PIM-1 were predicted. The study of the radial distribution functions revealed that the nitrogen atoms of PIM-1 were the preferential interaction sites with methanol molecules. The latter also had favorable interactions with the aromatic rings of PIM-1 through hydrogen bond-like interactions. These results cannot be transfered to other OSN polymer such that PI and PDMS. Indeed, PIM-1 showed high permeance in apolar solvents and alcohols in comparison

with PI [7] suggesting different molecular interactions. Furthermore, PI, PIM-1 (glassy polymers) and PDMS (rubbery polymer) are polymers with different chain rigidity, which have all shown different performance in OSN[3]. Eventually, PIM-1 is characterized by ultrahigh free volume contrary to PI and PDMS, which exhibit denser structures. For all these reasons the interactions between methanol/toluene binary mixtures and these three polymers are most probably different and need additional investigations. This study paves the way to a better understanding at the microscopic scale of membrane separations in OSN.

Competing Financial Interest

The authors declare no competing financial interests.

Acknowledgements

We are grateful to the ANR for its financial support through the project "MANIAC" (ANR-18-CE07-0028-02).

References

References

[1] C. Castel, E. Favre, Membrane separations and energy efficiency, J. Mem. Sci. 548 (2018) 345–357.

[2] R.P.Lively, D. Sholl, From water to organics in membrane separations, Nat. Mater. 16 (3) (2017) 276–279.

[3] P. Marchetti, M. J. Solomon, G. Szekely, A. Livingston, Molecular separation with organic solvent nanofiltration: a critical review, Chem. Rev. 114 (2014) 10735–107806.

[4] R. Gould, L. White, C. Wildemuth, Membrane separation in solvent lube dewaxing, Environ. Prog. 20 (1) (2001) 12–16.

[5] S. Darvishmanesh, L. Firoozpour, J. vanneste, P. Luis, J. Degrève, B. V. der Bruggen, Performance of solvent resistant nanofiltration membranes for purification of residual solvent in the pharmaceutical industry: experiments and simulation, Green Chem. 13 (2011) 3476–3483.

[6] A. Keraani, T. Renouard, C. Fishmeister, C. Bruneau, M. Rabiller-Baudry, Recovery of enlarged olefin metathesis catalysts by nanofiltration in an eco-friendly solvent, ChemSusChem 1 (2008) 927.

[7] D. Fritsch, P. Merten, K. Heinrich, M. L. ans M. Priske, High performance organic solvent nanofiltration membranes: Development and thorough testing of thin film composite membranes made of polymers of intrinsic microporosity (pims), J. Mem. Sci. 401-402 (2012) 222–231.

[8] N. Chaukura, L. Maynard-Atem, Interaction of a polymer of intrinsic microporosity (pim-1) with penetrants, American Journal of Applied Chemistry 3 (3) (2015) 139.

[9] J. Liu, Q. Xu, J. Jiang, A molecular simulation protocol for swelling and organic solvent nanofiltration of polymer membranes, J. Mem. Sci. 573 (2019) 639–646.

[10] Q. Xu, J. Jiang, Effects of functionalization on the nanofiltration performance of pim-1: Molecular simulation investigation, J. Mem. Sci. 591 (2019) 117357.

[11] P. Marchetti, A. Livingston, Predictive membrane transport models for organic solvent nanofiltration: How complex do we need to be?, J. Mem. Sci. 476 (2015) 530–553.

[12] S. Yuan, J. Wang, X. Li, J. Zhu, A. Volodine, X. Wang, J. Yang, P. V. Puyvelde, B. V. der Bruggen, New promising polymer for organic solvent nanofiltration: Oxidized poly (arylene sulfide sulfone), J. Mem. Sci. 549.

[13] Q. Xu, J. Jiang, Computational characterisation of ultrathin polymer membranes in liquids, Macromolecules 51 (2018) 7169–7177.

[14] Q. Xu, J. Jiang, Molecular simulations of liquid separations in polymer membranes, Current Opinion in Chem. Eng. 28 (2020) 66–74.

[15] I. Essafri, A. Ghoufi, Microstructure of nonideal methanol binary liquid mixtures, Phys. Rev. E 99 (6) (2019) 062607.

[16] R. Swaidan, B. Ghanem, E. Litwiller, I. Pinnau, Physical aging, plasticization and their effects on gas permeation in rigid polymers of intrinsic microporosity, Macromolecules 48 (2015) 6553–6561.

[17] P. Bernardo, F. Bazzarelli, F. Tasseli, G. Clarizia, C. Mason, L. Maynard-Atem, P. Budd, M. Lanc, K. Pilnacek, O. Vopicka, K. Friess, D. Fritsch, Y. Yampolskii, V. Shantarovich, J. Jansen, Effect of physical aging on the gas transport and sorption in pim-1 membranes, Polymer 113 (2017) 283–294.

[18] R. Hou, S. Smith, C. Wood, R. Mulder, C. H. Lau, H. Wang, M. R. Hill, Solvation effects on the permeation and aging performance of pim- 1-based mmms for gas separation, ACS Appl. Mater. & Interfaces 11 (2018) 6502.

[19] F. Almansour, M. Alberto, R. S. Bhavsar, X. Fan, P. M. Budd, P. Gorgojo, Recovry of free volume in pim-1 membranes through alcohol vapor treatment, Front. Chem. Sci. Eng. 154 (4) (2021) 872–881.

[20] W. Ogieglo, K. Rahimi, S. B. Rauer, B. Ghanem, X. Ma, I. Pinnau, M. Wessling, How do organic vapors swell ultrathin films of polymer of intrinsic microporosity pim-1, J. Phys. Chem. B 121 (2017) 7210–7220.

[21] W. Ogieglo, B. Ghanem, X. Ma, I. Pinnau, M. Wessling, How much do ultrathin polymers with intrinsic microporosity swell in liquids?, J. Phys. Chem. B 120 (2016) 10403–10410.

[22] L. Abbott, J. Hughes, C. Colina, Virtual synthesis of thermally cross-linked copolymers from a novel implementation of polymatic, J. Phys. Chem. B 118 (2014) 1916–1924.

[23] S. Plimton, Fast parallel algorithms for short range molecular dynamics, J. Comp. Phys. 117 (1995) 1–19.

[24] G. Larsen, P. Lin, K. Hart, C. Colina, Molecular simulations of pim-1-like polymers of instrinsic microporosity, Macromolecules 44 (2011) 6944–5951.

[25] P. Budd, E. Elabas, B. Ghanem, S. Makhseed, N. McKeown, K. Msayib, C. Tattershall, D. Wang, Solution-processed organophilic membrane derived from a polymer of intrinsic microporosity, Adv. Mater. 16 (2004) 456–459.

[26] D. Hofmann, L. Fritz, J. Ulbrich, C. Schepers, M. Bohning, Detailed-atomistic molecular modeling of small molecule diffusion and solution processes in polymeric membrane materials, Macromol. Theory Simul. 9 (2000) 293.

[27] J. Wang, R. Wolf, J. Caldwell, P. Kollman, D. Case, Development and testing of a general amber force field, J. Comp. Chem. 25 (2004) 1157–1174.

[28] H. Frentrup, K. Hart, C. Colina, E. Muller, In silico determination of gas permeabilities by non-equilibrium molecular dynamics: Co2 and he through pim-1, Membranes 5 (2015) 99–119.

[29] R. Semino, N. Ramsahye, A. Ghoufi, G. Maurin, Microscopic model of the metal-organic framework/polymer interface: A first step toward understanding the compatibility in mixed matrix membranes, ACS Appl. Mater. & Interfaces 8 (1) (2016) 809–819.

[30] W. Jorgensen, D. Maxwell, J. Tirado-Rives, Development and testing of the opls all-atom force field on conformational energetics and properties of organic liquids, J. Am. Chem. Soc. 118 (1996) 11225.

[31] A. Ghoufi, D. Morineau, R. Lefort, I. Hureau, L. Hennous, H. Zhu, A. Szymczyk, P. Malfreyt, G. Maurin, Molecular simulations of confined

liquids: An alternative to the grand canonical monte carlo simulations, J. Chem. Phys 134 (2011) 074104.

[32] M. Ding, A. Szymczyk, A. Ghoufi, Hydration of a polyamide reverse-osmosis membrane, J. Mem. Sci. 501 (2016) 248.

[33] P. Ewald, Die berechnung optischer und elektrostatischer gitterpotentiale, Ann. Phys. 64 (1921) 253.

[34] T. Darden, L. Perera, L. Pedersen, New tricks for modelers from the crystallography toolkit: the particle mesh ewald algorithm and its use in nucleic acid simulations, Structure 7 (1999) R55.

[35] W. Hoover, Canonical dynamics: Equilibrium phase-space distributions, Phys. Rev. A 31 (1985) 1695.

[36] T. Willems, C. Rycroft, M. Kazi, J. Meza, M. Haranczyk, Algorithms and tools for high-throughput geometry- based analysis of crystalline porous materials, Micr. Meso. Mater. 149 (2012) 134–141.

[37] C. Staiger, S. Pas, A. Hill, C. Cornelius, Gas separation, free volume distribution,and physical aging of a highly microporous spirobisindane polymer., Chem. Mater. 20 (2008) 2606–2608.

[38] N. McKeown, P. Budd, Exploitation of intrinsic microporosity in polymer-based materials, Macromolecules 43 (2010) 5163–5176.

[39] M. heuchel, D. Fritsh, P. Budd, N. McKeown, D. Hofmann, Atomistic packing model and free volume distribution of a polymer with intrinsic microporosity (pim-1), J. Mem. Sci. 318 (1) (2008) 84–99.

[40] M. Ferrario, M. Evans, Molecular dynamics computer simulation of liquid dichloromethane. i. equilibrium properties, chem. Phys. 72 (1982) 141–145.

[41] A. Luzar, D. Chandler, Effect of environnement on hydrogen bond dynamics in liquid water, Phys. Rev. letters 76 (1996) 928.

[42] M. D. Guiver, Y. Lee, Polymer rigidity improves microporous membranes, Science 339 (2013) 284–285.

[43] A. Ghoufi, I. Hureau, D. Morineau, R. Renou, A. Szymczyk, Confinement of tert-butanol nanoclusters in hydrophilic and hydrophobic silica nanopores, J. Phys. Chem. C 117 (2013) 15203.

[44] S. Stoddard, Identifying clusters in computer experiments on systems of particles, J. Comp. Physics 27 (2) (1978) 291.

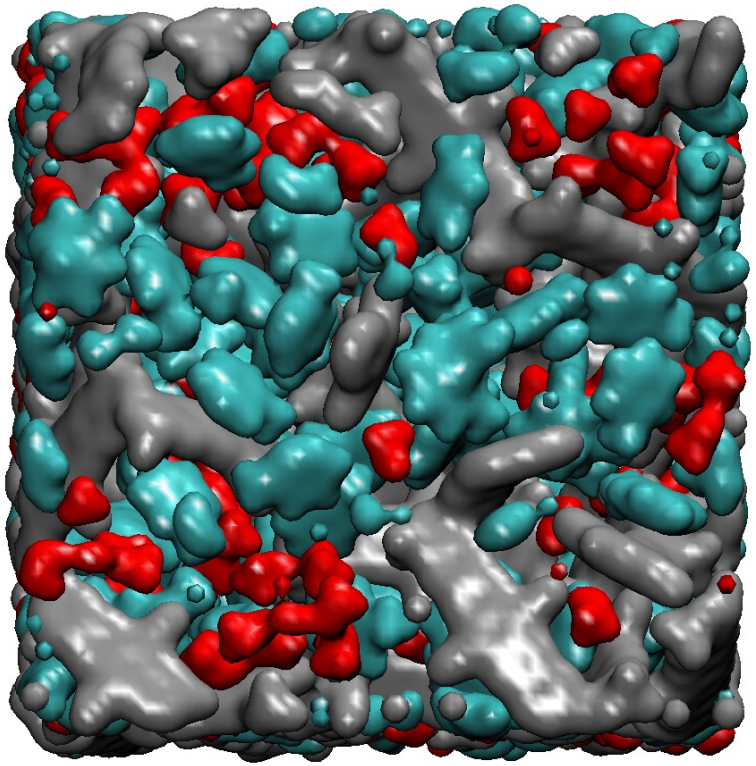

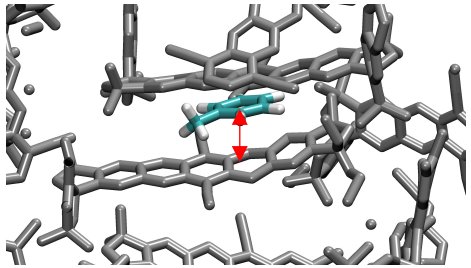

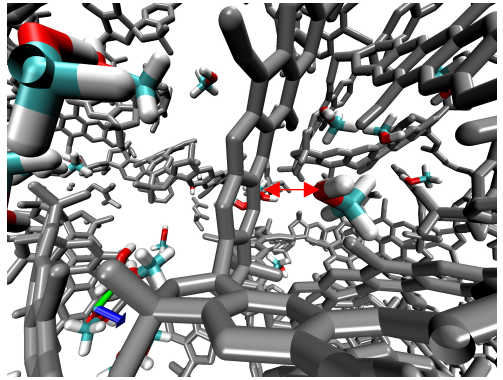

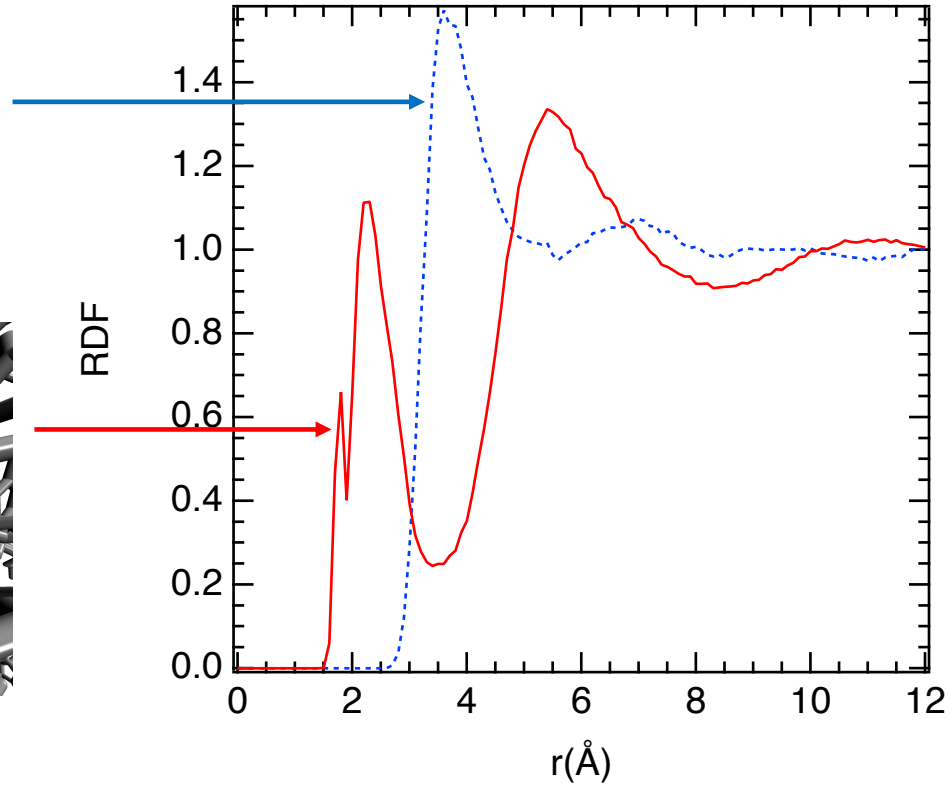

PIM-1 Methanol Toluene